Spin currents during ultrafast demagnetization of ferromagnetic bilayers

2017 J. Phys.: Condens. Matter 29 384002

(http://iopscience.iop.org/0953-8984/29/38/384002)

IOP Publishing Journal of Physics: Condensed Matter
J. Phys.: Condens. Matter **29** (2017) 384002 (8pp) https://doi.org/10.1088/1361-648X/aa7dd3

Spin currents during ultrafast demagnetization of ferromagnetic bilayers

A Eschenlohr[1], L Persichetti[2], T Kachel[3], M Gabureac[2,4], P Gambardella[2] and C Stamm[2]

[1] Fakultät für Physik, Universität Duisburg-Essen, Lotharstr. 1, 47057 Duisburg, Germany
[2] Department of Materials, ETH Zurich, CH-8093 Zurich, Switzerland
[3] Institut für Methoden und Instrumentierung der Forschung mit Synchrotronstrahlung, Helmholtz-Zentrum Berlin für Materialien und Energie GmbH, Albert-Einstein-Str. 15, 12489 Berlin, Germany

E-mail: andrea.eschenlohr@uni-due.de and christian.stamm@mat.ethz.ch

Received 15 January 2017, revised 5 July 2017
Accepted for publication 5 July 2017
Published 17 August 2017

Abstract

Ultrafast spin currents induced by femtosecond laser excitation of ferromagnetic metals have been found to contribute to sub-picosecond demagnetization, and to cause a transient enhancement of the magnetization of the bottom Fe layer in a Ni/Ru/Fe layered structure. We analyze the ultrafast magnetization dynamics in such layered structures by element- and femtosecond time-resolved x-ray magnetic circular dichroism, for different Ni and Fe layer thicknesses, Ru and Ta interlayers, and by varying the pump laser fluence. While we do not observe the transient enhancement of the magnetization in Ni/Ru/Fe discovered previously, we do find a reduced demagnetization of the Fe layer compared to a Ni/Ta/Fe layered structure. In the latter, the spin-scattering Ta layer suppresses spin currents from the Ni layer into Fe, consistent with previous results. Any spin current arriving in the lower Fe layer will counteract other, local demagnetization mechanisms such as phonon-mediated spin-flip scattering. We find by increasing the Ni and Fe layer thicknesses in Ni/Ru/Fe a decreasing effect of spin currents on the buried Fe layer, consistent with a mean free path of the laser-induced spin currents of just a few nm. Our results suggest that in order to utilize ultrafast spin currents in an efficient manner, the sample design has to be optimized with these considerations in mind, and further studies clarifying the role of interfaces in the employed layered structures are needed.

Keywords: ultrafast magnetization dynamics, laser-induced spin currents, x-ray magnetic circular dichroism, time-resolved x-ray spectroscopy

(Some figures may appear in colour only in the online journal)

1. Introduction

Ultrafast magnetization dynamics, i.e. the sub-picosecond (ps) dynamics of the magnetization of a ferro-, ferri- or antiferromagnetic material after femtosecond (fs) laser excitation [1–3], has received considerable attention as a means to study the fundamental microscopic processes in the interaction of a laser pulse with a magnetic material and as the basis for potential future magnetic recording schemes with writing times in the fs to ps range. Only recently the transport of angular momentum, or spin, was added to a range of other possible mechanisms to decrease the magnetization of a material on an ultrafast time scale. A fs laser pulse thereby initiates fs spin transport in the ballistic to diffusive range, leading to the ultrafast demagnetization of ferromagnets, as discussed in experimental work [4–7], and described by the superdiffusive transport model [8, 9]. The concept of ultrafast spin currents has recently been used to explain the transient, ultrafast enhancement of the magnetization in magnetic bilayers [10, 11], excite magnetization precession via spin-transfer torque [12], and influence the demagnetization in a magnetic tunnel

[4] Now at: Bern University of Applied Sciences, 2501-Biel-Bienne, Switzerland

junction under an applied bias voltage [13]. These observations show the potential for ultrafast spintronics applications, in which the magnetization of one layer or component can be manipulated by the injection of transient spin currents generated in another layer. However, open questions remain regarding the efficiency of spin current generation after laser excitation, compared to competing microscopic processes such as phonon-mediated spin-flip scattering [14], and their transport properties such as their effective mean free path.

Here, we focus in particular on ferromagnetic (FM) bilayers, with an interlayer allowing for both parallel and antiparallel alignment of the layers' magnetization by means of indirect exchange coupling, depending on the applied magnetic field. In such a layered structure, namely Ni/Ru/Fe, a transient enhancement of the magnetization of the bottom Fe layer due to superdiffusive spin currents from the top Ni layer was first observed by Rudolf *et al* [10]. This behavior is argued to be the signature of a spin current from the laser irradiated top layer into the lower layer, and lastly is a consequence of angular momentum conservation during ultrafast demagnetization. The effect was found to occur in a particular pump fluence range, and for a parallel orientation of the Ni and Fe layers' magnetization. Moreover, the laser-induced spin current was observed to be directional, from the top Ni to the bottom Fe layer, and could be suppressed by choosing a spin-scattering or insulating interlayer instead of Ru [11]. The aforementioned results were obtained in transversal magneto-optical Kerr effect (MOKE) measurements, resonant with the shallow core level *M*-edges of Ni and Fe to achieve element- and thus layer-sensitivity, employing ultrashort vacuum ultraviolet (VUV) pulses from a high harmonic generation (HHG) source. A subsequent investigation using time-resolved MOKE in the visible wavelength range on similar samples [15], where the layer sensitivity was derived from exploiting different combinations of the Kerr ellipticity and rotation, did not observe a transient magnetization enhancement in Fe, as the experiment was performed at a lower pump fluence, where no transient magnetization enhancement would be expected according to [10, 11], but estimated the contribution of spin currents to the demagnetization at about 30%. As these studies show, a full understanding of the ultrafast spin dynamics in ferromagnetic bilayers remains challenging.

We aim to shine new light on the ultrafast magnetization dynamics in FM bilayers by employing a complementary experimental technique, fs time-resolved x-ray magnetic circular dichroism (XMCD) at the Ni and Fe *L*-edges in the soft x-ray range. Both the visible and VUV MOKE require that the bottom FM layer is accessible to the probe, which has a similar penetration depth as the pump (on the order of 15 nm). Employing soft x-rays with a higher penetration depth, and performing a transmission measurement as sketched in figure 1, we efficiently probe the sample in its full thickness. Furthermore, as XMCD is an element-sensitive technique, the dynamic response of the magnetic layers is probed individually, provided that the layers consist of different elements. These advantages allow us to study the interplay between direct optical excitation and spin transport by varying the FM layer thicknesses in a Ni/Ru/Fe layered

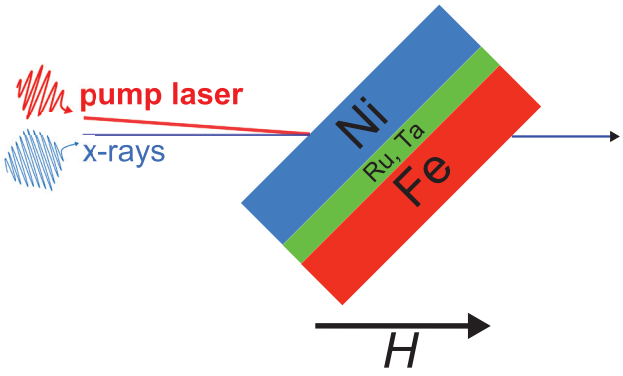

Figure 1. Schematic depiction of the XMCD measurement geometry. For the time-resolved measurements, a near-infrared laser pump pulse impinges nearly collinearly with the 100 fs soft x-ray probe pulse on the Ni/Ru/Fe or Ni/Ta/Fe layered structures. The x-ray absorption for parallel and antiparallel orientation of the applied magnetic field *H* with respect to the x-ray propagation direction is acquired by measuring the transmitted x-ray intensity.

structure. We thus extend the thickness range to larger values not previously covered by [10, 11, 15]. We furthermore investigate the possible influence of the interlayer material by changing it from Ru to Ta. From our analysis of the element-resolved dynamics in Ni/Ru/Fe, we find almost no demagnetization and no transient magnetization enhancement in 15 nm thick Fe for a 15 nm thick Ni top layer, for parallel Ni and Fe magnetization direction and independent of the pump fluence. Also for Ni/Ru/Fe with a 5 nm (4 nm) thick Ni (Fe) layer, the same sample structure as in [10, 11], apart from the buffer layer, no magnetization enhancement is observed in the investigated fluence range, in agreement with [10]. Differences in the ultrafast magnetization dynamics between samples with Ru and Ta interlayers are small but consistent with the previously found suppression of spin currents by the Ta interlayer [11]. We discuss our results in the context of two superimposed and possibly competing effects, local demagnetization by optical excitation, and non-local spin currents between the layers. Our results argue for a limited mean free path of superdiffusive spin currents.

2. Method

Our samples were prepared by magnetron sputtering on Si_3N_4 membranes with a 200 nm thick Al heat sink deposited on the back of the membrane. From the top (capping) to the bottom (seed) layer, the layer orders and thicknesses are the following: Al 3 nm/Ni 15 nm/Ru 1.5 nm/Fe 15 nm/Ru 5 nm (labeled in the following as 'Ru1'), Al 3 nm/Ni 5 nm/Ru 1.5 nm/Fe 4 nm/Ru 5 nm ('Ru2') and Al 3 nm/Ni 5 nm/Ta 2 nm/Fe 4 nm/Ta 3 nm ('Ta').

In order to characterize our samples, static x-ray absorption spectroscopy (XAS) and XMCD measurements were performed at the PM3 beamline of the BESSY II electron storage ring operated by Helmholtz Zentrum Berlin. The absorption of circularly polarized x-rays resonant with the Ni and Fe *L*-edges ($2p \rightarrow 3d$ transitions) was measured in transmission geometry for opposite orientations of the applied

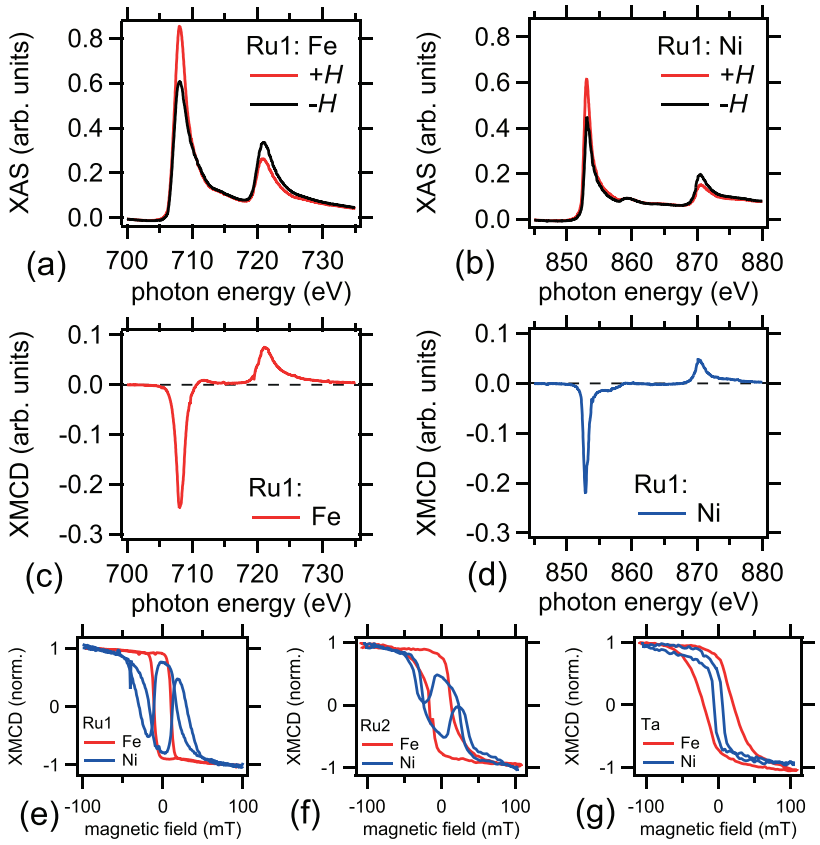

Figure 2. X-ray absorption spectra of the Ru1 sample using circularly polarized x-rays at the Fe (a) and Ni (b) *L* absorption edges, for opposite directions of the applied magnetic field $H = \pm 0.39$ T oriented parallel to the x-ray propagation direction. The resulting XMCD for the Ru1 sample is displayed in (c) and (d), while element-resolved hysteresis loops are shown in (e)–(g) for all three samples.

magnetic field, which was chosen large enough to align the Ni and Fe magnetization directions parallel to each other and saturate the sample's magnetization. Since we measure with XMCD the projection of the magnetization on the x-ray propagation direction, and the sample is magnetized in-plane, the incidence angle between the surface normal and the x-ray propagation direction was set to 35°. Exemplary static XAS and XMCD spectra are displayed in figures 2(a)–(d). We furthermore acquired element-resolved hysteresis loops by setting the x-ray energy to the maximum XMCD at the Ni L_3-edge at 853 eV or respectively to the Fe L_3-edge at 708 eV, see figures 2(e)–(g). The hystereses for the Ru1 and Ru2 samples demonstrate the antiparallel alignment of the Ni and Fe layers' magnetization in zero magnetic field, and the parallel alignment when the field is increased, compare figures 2(e) and (f), due to indirect exchange coupling via the Ru interlayer. This behavior does not occur for the Ta sample, see figure 2(g).

Femtosecond time-resolved measurements were carried out at the UE56/1-ZPM beamline of the BESSY II Femtoslicing facility [16, 17]. In a pump-probe experiment, circularly polarized soft x-rays with 100 fs pulse length are generated at a repetition rate of 6 kHz, while 50 fs short laser pulses at 780 nm central wavelength (1.55 eV photon energy) and 3 kHz repetition rate are used for pumping the sample. Since the pump and probe pulses are both generated from the same Ti:sapphire oscillator, they are intrinsically synchronized in a jitter-free manner, which results in an overall time resolution of 130 fs [17, 18]. Laser pump and x-ray probe pulses coincide on the sample in an almost collinear geometry (<1.5°), as drawn in figure 1. The transmitted x-rays are detected using an avalanche photodiode and time gated using a boxcar integrator, thus acquiring alternately the pumped and unpumped XAS/XMCD signals. As in the static measurements, the angle of incidence was 35°. All time-resolved measurements were performed for parallel orientation of the Ni and Fe layers' magnetization in an external field of 0.12 T for Ru1, and 0.24 T for Ru2 and Ta samples. The same relative orientation was used when the transient magnetization enhancement was observed [10, 11].

The magnetization dynamics in the Ni layer are investigated by setting the x-ray energy to the maximum Ni XMCD signal, i.e. to the Ni L_3-edge at 853 eV. Respectively, the Fe magnetization dynamics are observed at the Fe L_3-edge at 708 eV. Since we effectively integrate over the whole L_3-edge due to a limited energy resolution of about 3 eV in the fs time-resolved measurements, the measured XMCD signal represents a linear combination of spin and orbital angular momenta according to the XMCD sum rules [18–20]. The pump spot radius was approximately 600 μm, which results in an incident pump fluence of 3.5–21 mJ cm^{-2} for an average pump power of 10–60 mW. We estimate the uncertainty in the pump fluence to be about ± 30 %, due to uncertainties in the determination of the exact pump spot size and shape.

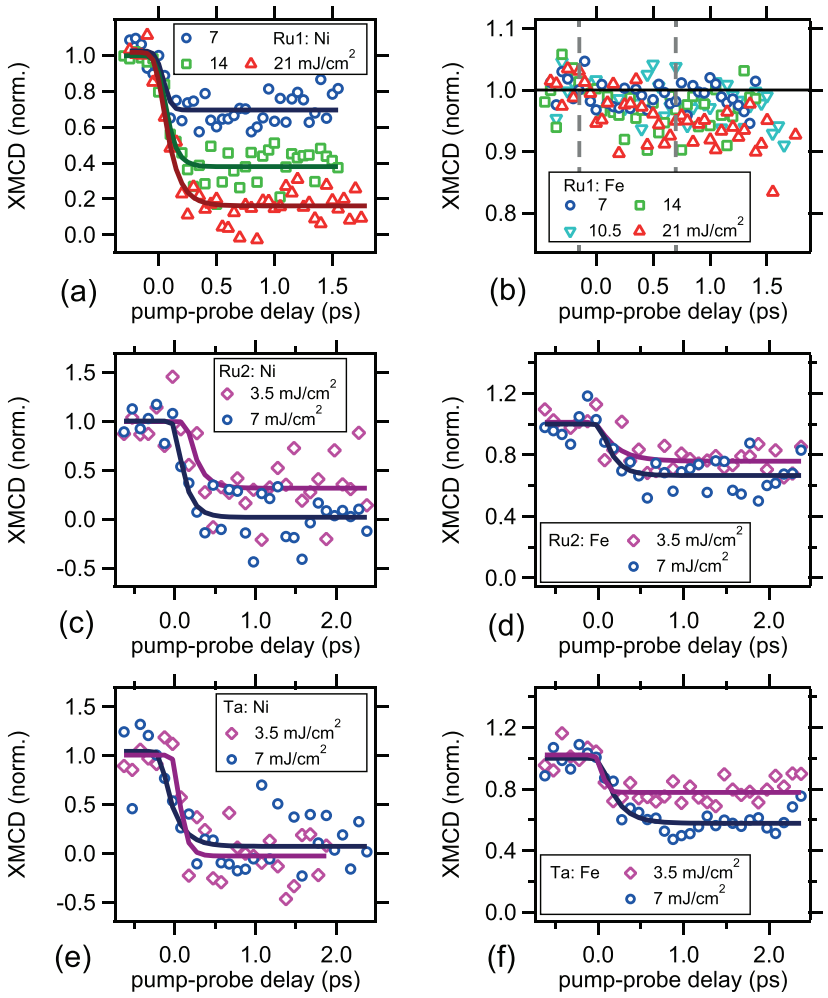

Figure 3. Time-resolved XMCD normalized to their values before laser excitation as function of the pump-probe time delay (symbols). Ni (a) and Fe (b) layers of the Ru1 sample, Ni (c) and Fe (d) layers of the Ru2 sample, and Ni (e) and Fe (f) layers of the Ta sample, for different pump fluences as indicated. Solid lines are fits to the data according to equation (1).

3. Results

We first take a look at the time-dependent XMCD on the Ru1 sample with 15 nm thick Ni and Fe films, displayed in figures 3(a) and (b). For the Ni layer, the L_3 edge XMCD signal decreases rapidly in the first $\approx$300 fs and then stays at a practically constant value within the measured time window of 1.5 ps, before relaxation to the equilibrium value occurs on timescales of several hundreds of ps (not shown). With increasing pump fluence, the Ni layer demagnetizes more strongly, from about $30 \pm 10\%$ at a pump fluence of 7 mJ cm^{-2} to about $80 \pm 10\%$ at 21 mJ cm^{-2}. In order to describe our results in a more quantitative manner, we fit the time-dependent XMCD curves for $t > 0$ with the function

$$f(t) = G(t) \otimes (1 - \Delta A \cdot \mathrm{e}^{-\tau/t}) \qquad (1)$$

i.e. a single exponential decay convoluted with a Gaussian $G(t)$ representing the experimental time resolution of 130 fs. ΔA is the normalized magnitude of demagnetization and τ its time constant. The summary of the fit results displayed in figure 4(a) indicates that ΔA for Ni increases almost linearly with increasing pump fluence. Also for τ, compare figure 4(b), a clear increase with increasing pump fluence is observed, for example, τ more than doubles, from about 70 fs to 160 fs, for an increase of the pump fluence from 14 to 21 mJ cm^{-2}.

In contrast to the Ni layer, the normalized XMCD signal of the Fe layer displayed in figure 3(b) shows little change after laser excitation even for the maximum pump fluence. No transient enhancement of the magnetization, but instead a small demagnetization on the order of a few percent is observed. As the limited data quality due to these very small transient changes did not allow for a fit to the Fe data according to equation (1) with reasonable accuracy, we determined ΔA by taking the difference of the average values of the normalized XMCD before zero delay and after 0.7 ps, respectively, as indicated by the dashed vertical lines in figure 3(b). As can be seen in figure 4(a), ΔA for the Fe layer slightly increases, from approximately 1% to 8% for the highest pump fluence used. Due to the small ΔA, the Fe demagnetization time constant can only be estimated to be $\tau \approx 0.1$–1 ps.

Now we turn our attention to the samples with thinner Ni and Fe layers. For a pump fluence of 7 mJ cm^{-2}, the Ni layer in the Ru2 sample shows close to total demagnetization, see figure 3(c). The amount of demagnetization of Ni is reduced

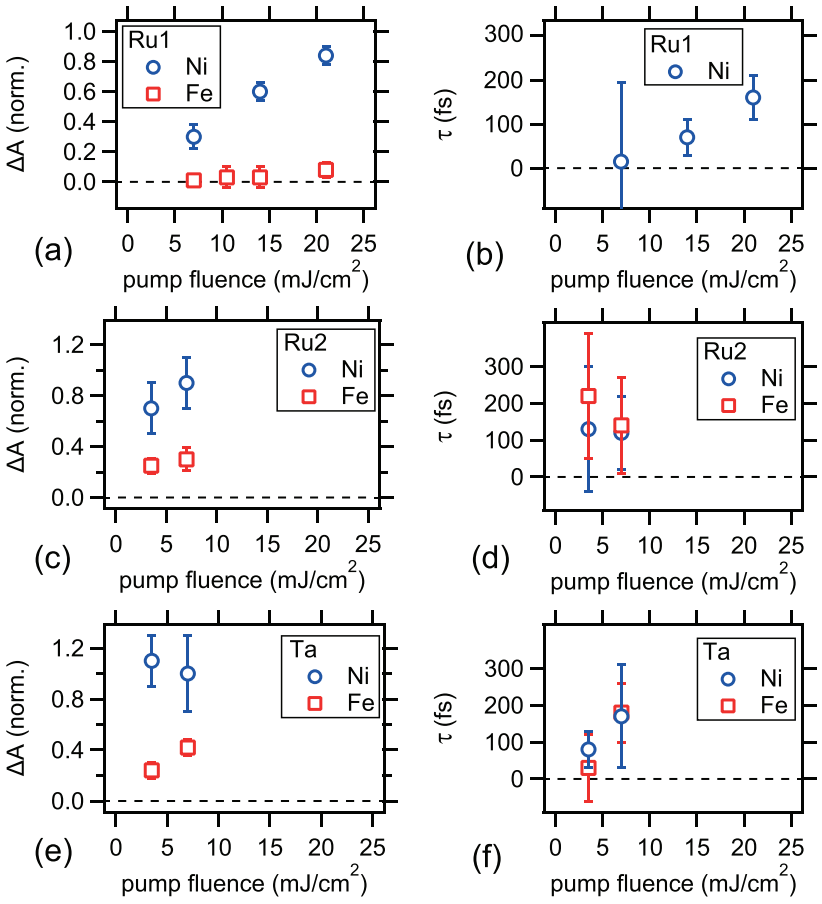

Figure 4. Fit results according to equation (1). Normalized demagnetization strength ΔA for Ru1 (a), Ru2 (c), and Ta samples (e), and demagnetization time constants τ for Ru1 (b), Ru2 (d), and Ta (f) samples as function of the pump fluence. Error bars indicate the standard deviation.

to about $70 \pm 20\%$ for a pump fluence of 3.5 mJ cm^{-2}. As can be seen in figure 3(d), the Fe layer shows for both pump fluences a clear demagnetization. The fluence dependent difference in the demagnetization of the Fe layer is very small.

The time-dependent XMCD of the Ta sample is displayed in figures 3(e) and (f). The Ni layer of the Ta sample in figure 3(e) shows almost 70–100 % demagnetization for a pump fluence of 7 mJ cm^{-2}, similar to the Ru2 sample. In contrast to the latter sample, here the demagnetization is practically the same also for a reduced fluence of 3.5 mJ cm^{-2}. As figure 3(f) indicates, the Fe layer of the Ta sample also shows an ultrafast demagnetization. In contrast to the Ru2 sample, a significant fluence-dependent difference in the Fe demagnetization is observed, namely $42 \pm 6\%$ demagnetization for a pump fluence of 7 mJ cm^{-2} compared to $24 \pm 6\%$ for 3.5 mJ cm^{-2}. Moreover, for 7 mJ cm^{-2} pump fluence the amount of Fe demagnetization is clearly higher in the Ta sample than in the Ru2 sample.

The fit results according to equation (1) for the Ru2 and Ta samples are summarized in figures 4(c)–(f). The demagnetization time constants τ, shown in figures 4(d) and (f), are similar for both samples and both the Ni and Fe layers, considering the error bars, and range between 50 fs and 250 fs. Only one data point hints at a different behavior of the two samples: when comparing τ of Fe for the lower fluence, it is higher in Ru2 than in the Ta sample. The fluence-dependent behavior of ΔA, plotted in figures 4(c) and (e), corroborates differences in the samples' individual dynamic responses. In particular, a stronger demagnetization of the Fe layer with increasing pump fluence is observed in the Ta sample compared to the Ru2 sample, and the Ni layer of the Ru2 sample

Table 1. Comparison of our Ru1, Ru2 and Ta samples to the samples of [10, 11], for the cases where the sample structures and excitation conditions are most closely matched, or for the lowest pump fluence in case of our Ta sample. d_{Ni}, d_{Ru}, d_{Ta} and d_{Fe} refer to the thicknesses of the Ni, Ru, Ta and Fe layers, respectively. ΔA_{Ni} (ΔA_{Fe}) is the amount of demagnetization of the Ni (Fe) layer. Note that the negative value of ΔA_{Fe} for the sample from [11] indicates a transient enhancement of the magnetization according to our definition of ΔA in equation (1). 'exc. ratio' refers to the relative optical excitation of the Ni compared to the Fe layer.

Sample	d_{Ni} (nm)	d_{Ru} (nm)	d_{Ta} (nm)	d_{Fe} (nm)	ΔA_{Ni} (%)	ΔA_{Fe} (%)	Exc. ratio
Ru1	15	1.5	—	15	60 ± 6	≈ 7	1.9
Ru2	5	1.5	—	4	70 ± 20	25 ± 6	1.3
[10]	5	1.5	—	4	≈ 70	≈ 15	—
[11]	5	1.7	—	4	68 ± 1	-16 ± 1	1.2
Ta	5	—	2	4	110 ± 20	24 ± 6	1.4
[11]	5	—	2	4	55 ± 2	13 ± 1	1.2

shows a weaker demagnetization at lower pump fluence than the Ni layer in the Ta sample. In the following, we discuss these observations in context with previous results [10, 11, 15]. We summarize our findings, in comparison with those of [10, 11], in table 1.

4. Discussion

We do not observe a transient enhancement of the Fe magnetization, as found previously in similar Ni/Ru/Fe layered structures [10, 11], in either of our samples with a Ru interlayer. One possible reason for this are different pumping conditions in our experiment compared to [10, 11], i.e. how strongly the Ni layer is excited and thus how many excited carriers can contribute to the spin current into the Fe layer. In [10], the transient magnetization enhancement was found to occur only in an intermediate fluence range, with the spin current being rather weak at low pump fluence, and the magnetization enhancement not occurring above a particular pump fluence. The optimal conditions for the magnetization enhancement corresponded to about 30–50% demagnetization in the Ni layer [10]. In the Ru1 sample, we achieve approx. 30–60% Ni demagnetization in the 7–14 mJ cm^{-2} fluence range, and yet no transient enhancement of the Fe magnetization is observed for this sample with thicker layers in comparison to the sample in [10]. While the error bars of ΔA would in principle support a magnetization increase smaller than 4% (compare figure 4(a)), a 10–20% increase would be expected according to [10], based on the amount of the Ni demagnetization. However, the amount of Ni demagnetization is not the only factor that affects the transient magnetization in the Fe layer.

To discuss this point more in detail, we now turn our attention to the Ru2 sample with ferromagnetic layers of the same thickness as in [10, 11]. The laser excitation of this sample results in a Ni demagnetization of $70 \pm 20\%$ and a Fe demagnetization of $25 \pm 6\%$, for the lower fluence. These values agree quite well with [10], supplementary figure S2(c), where a decrease of the Ni magnetization of $\approx$70% is accompanied by a Fe demagnetization of $\approx$15%. The above values for the Ni demagnetization are also close to the one found in [11] for a Ni/Ru/Fe sample with slightly thicker (1.7 nm) Ru interlayer, which however lead to a 16% Fe layer magnetization increase, compare table 1. This indicates that besides the amount of demagnetization of the upper layer, additional parameters are needed to describe the magnetization dynamics in ferromagnetic bilayer samples.

In the following, we discuss the possible influence of two factors. First, we will consider the relative strength of the optical excitation in the Ni layer compared to the Fe layer. The direct optical excitation of the Fe layer correlates with the local loss of spin polarization due to spin-flip scattering processes of the hot carriers [14]. The effect of these local spin-flips can be counteracted by non-local spin currents coming from the Ni layer [10, 11, 15]. The relative optical excitation of the Ni compared to the Fe layers is thus related to the interplay between the strength of the laser-induced spin current in Ni versus the loss of spin polarization by directly exciting the Fe layer. Second, we also discuss the sample structure, especially the layer thicknesses, which may potentially limit the influence of spin transport in case they are larger than the spin current mean free path.

We begin by looking at the interplay of the local demagnetization by optical excitation and non-local spin currents, which can be discerned by comparing the effects of the optical excitation on the Ni and Fe layers. In the Ni layer, a stronger excitation will cause a stronger spin current traveling into the Fe layer. This spin current will contribute to the demagnetization of the Ni layer. In the Fe layer, a stronger optical excitation will lead to a loss of spin polarization due to spin-flip scattering processes, e.g. phonon-mediated spin flips as demonstrated in [14], which are proportional to the strength of optical excitation as measured by the electron temperature. These spin-flip processes thus lead to a demagnetization of the Fe layer. A magnetization enhancement of the Fe layer as observed in [10, 11], or a reduced demagnetization, is achieved by the counteracting influence of spin currents from the Ni layer. Note that we assume the spin currents to be directional, from the Ni to the Fe layer only (not the other way around), as demonstrated in [11]. In order to discern the potential influence of the relative strength of pump pulse absorption in the different FM layers, we therefore calculate the layer-resolved absorption with the aid of the IMD software [21] and the procedure employed in [22]. For the Ru2 sample, we derive an absorption in the Ni layer of 18% of the total absorption in the sample structure (excluding the substrate and the metallic heat sink on the back of the substrate) and 14% in the Fe layer, which means that the Ni layer is 1.3 times more strongly excited than the Fe layer. In the corresponding sample with a Ru interlayer and the same Ni and Fe layer thicknesses in [11], in which a transient magnetization enhancement was observed, the absorption ratio of the Ni compared to the Fe layer was given as 1.2 (supplemental material of [11]). We expect the same absorption ratio for the sample in [10], where a Fe layer demagnetization in good agreement with our observation on the Ru2 sample was found, as 0.2 nm less of Ru (on the order of one monolayer) is not expected to significantly alter the optical absorption. These are practically the same relative excitation conditions as in our Ru2 sample, so that our results can be compared to [10, 11].

With regard to the potential effect of the sample structure, i.e. the thickness of the Ni and Fe layers, we estimate the effective mean free path (MFP) of the laser-induced spin current in Ni and Fe. In the ferromagnetic transition metals, the spin-dependent inelastic MFPs of electrons in the range of up to 1.5 eV above the Fermi level are on the order of a few nm [23, 24]. The ratio of the MFPs of majority compared to minority electrons is calculated to be about 4:1 in Fe and up to 8:1 in Ni [23, 24]. The difference in the mean free paths between majority and minority electrons is decisive for the effective reach of the ultrafast spin current, which represents a spatial redistribution of spin polarization. With a minority electron MFP on the order of 1 nm for both Ni and Fe [23, 24], and the respective majority:minority MFP ratios, we can thus estimate an effective MFP of the spin current in Fe of about 3 nm, and up to 7 nm in Ni. Note that the aforementioned

majority:minority lifetime and MFP ratios for Ni and Fe from theory [23, 24] are generally overestimated compared to experimental values, where the ratios are closer to 1.5–2:1 [25–27], so our estimate represents an upper boundary. This rough estimate is nevertheless consistent with previous theoretical [9] and experimental [28] investigations, where demagnetization by femtosecond spin transport into a conducting substrate was observed in a 5-6 nm wide region of the ferromagnet close to the substrate. Moreover, femtosecond laser-induced spin currents were also observed to penetrate about 2 nm into a Fe layer [29] and have an effective MFP of about 3 nm in Co [30]. Thus, we can now understand the different magnetization dynamics in the Ru1 and Ru2 samples. Noting that with time-resolved XMCD in transmission geometry, we probe the whole Ni and Fe layers at the respective L_3 edges, we explain the weaker magnetization changes of the Ru1 compared to the Ru2 sample for the same incident pump fluence, compare figures 4(a) and (c), with the fact that the demagnetization in the Ru1 sample is more spatially inhomogeneous. In the Ru1 sample with 15 nm thick Ni and Fe layers, the laser-induced spin current can neither escape from the surface region of the Ni layer nor fully penetrate into the Fe layer. In particular, the very small ΔA of Fe of only a few percent even for the highest pump fluence, see figure 4(a), results from the limited MFP of the spin current in Fe in combination with the weaker optical excitation of this layer. A fs spin current emanating from the top Ni layer can only affect the topmost ≈ 3 nm wide region of Fe, and thus no transient magnetization enhancement is observed when the whole film is probed. Also laser pulse induced spin-flip processes leading to a demagnetization [14] are less prominent in the Fe layer of the Ru1 compared to the Ru2 sample, as Fe is less strongly excited due to the optical absorption in the Ni layer being 1.9 times stronger than in the Fe layer, which is a consequence of the thicker Ni film. We conclude that ferromagnetic layer thicknesses that are matched to the effective MFP of laser-induced spin currents are essential in maximizing the effect of spin transport on the transient magnetization.

Furthermore, the morphology and quality of the interfaces in the sample structure might play an additional, important role which has so far not been systematically investigated for femtosecond spin transport, by altering the transport properties of the spin current transmitted through these interfaces. In particular, the interface properties (related to the preparation method) might explain the differences in the fluence dependence of the magnetization dynamics between otherwise similar samples, i.e. for a comparable 70 % demagnetization of the Ni layer in [10, 11] and our Ru2 sample, where the Fe layer magnetization enhancement was only observed in [11], compare table 1. As the importance of the interface for spin-dependent transport is already well documented for the giant magnetoresistance effect [31, 32], this warrants further time-resolved studies in the future, in which e.g. the interface quality is systematically varied. In bulk, the effect of lattice disorder on lattice-mediated spin-flip scattering, when spin currents are driven by THz pulses, has recently been identified [33].

Lastly, we evaluate the effect of the interlayer material on the spin current-induced contribution to the demagnetization in our ferromagnetic bilayer samples. For this, we compare the Ru2 and Ta samples, which have the same Ni and Fe layer thicknesses, respectively, but a different interlayer. Previous data demonstrated that a Ta interlayer efficiently inhibits spin currents between the Ni and Fe layers [11]. As for the laser excitation, we note that the Ni and Fe layers are subject to similar conditions for both samples. In the Ta sample, the Ni layer accounts for 29% of the total absorption in the sample structure compared to 21% for the Fe layer, leading to an absorption ratio of 1.4, similar to the ratio of 1.3 for the Ru2 samples derived above. Note that the different percentages of the absorption in the Ni (or respectively Fe) layers in the Ru2 compared to the Ta sample are because of the different absorption of the pump pulse in the Ru compared to the Ta inter- and seed layers. As shown in figure 4(e), the Fe demagnetization in the Ta sample for 7 mJ cm^{-2} is roughly 1.3 times stronger than that of the Ru2 sample. Under the assumption that spin transport from the Ni layer compensates local demagnetization in the Fe layer by i.e. phonon-mediated spin-flip scattering [14], our observation of a stronger demagnetization for an interlayer which inhibits spin transport is consistent with previous results [11]. This observation also allows us to estimate the relative contribution of spin currents to the magnetization dynamics in the bottom Fe layer. We make two assumptions, namely that the relative strength of spin transport compared to counteracting spin-flip processes is determined by the Ni:Fe layer absorption ratio of the pump pulse, as discussed above, which is practically the same for the Ru2 and Ta samples, and that the Ta interlayer suppresses spin transport between the Ni and Fe layers entirely. Then, we would expect the Ru2 sample to demagnetize 1.3 times stronger if the Ru interlayer would be replaced with Ta, which corresponds to a relative contribution of the spin currents of roughly 25% on the Fe magnetization dynamics by counteracting local spin-flips. Our results are in line with [15], where transport effects were shown to account for about 30% of the observed magnetization dynamics.

5. Conclusion

Based on element-sensitive time-resolved XMCD measurements performed resonantly at the L absorption edges of Ni and Fe, we have analyzed the layer-resolved ultrafast magnetization dynamics in Ni/Ru/Fe and Ni/Ta/Fe layered structures. In a Ni/Ru/Fe sample with 15 nm thick Ni and Fe layers, we find only a very small transient change of the magnetization in the bottom Fe layer for a pump fluence range in which the top, more strongly optically excited Ni layer is demagnetized between 30 and 80%. We explain this observation with the limited mean free path of only a few nm of the laser-induced spin currents launched in the top layer. A Ni/Ru/Fe sample with 5 nm thick Ni and 4 nm thick Fe layers, i.e. layer thicknesses below or on the order of the presumed spin current mean free paths, shows a stronger demagnetization of the Fe layer than the sample with thicker films. No transient increase of the magnetization is observed, but the results are in line with an equivalent sample structure for similar excitation conditions, measured by MOKE using VUV photons tuned to the M absorption edges [10]. The Ta interlayer of the

Ni/Ta/Fe sample is shown to suppress spin currents, consistent with previous findings [11], leading to a stronger local demagnetization of the Fe layer. An efficient utilization of laser-induced femtosecond spin currents thus requires a careful, systematic exploration of the apparently narrow parameter space in which a transient magnetization enhancement occurs. In particular, we point out the importance of sample structure optimization in order to match layer thicknesses to the spin current mean free path, and to ensure efficient laser excitation of the upper FM layer without too much affecting the lower FM layer. Additional studies are warranted on the effect of the interface morphology on the spin-dependent transport of laser-excited carriers, of which so far little is known.

Acknowledgments

We thank R Mitzner, N Pontius, and K Holldack for support during the time-resolved XMCD measurements, and C Schmitz-Antoniak, A Smekhova, N Svechkina and R Abrudan for support during the static XMCD experiments. Helmholtz Zentrum Berlin is gratefully acknowledged for the allocation of synchrotron radiation beamtime and for financial support for travel to BESSY II. L Persichetti acknowledges support from an ETH Postdoctoral Fellowship grant. This work was partially funded by the European Community's Seventh Framework Programme (FP7/2007-2013) under grant agreement n° 312284, and by the Swiss National Science Foundation, projects # 200021-153404 and 200020-172775.

References

[1] Beaurepaire E, Merle J-C, Daunois A and Bigot J-Y 1996 *Phys. Rev. Lett.* **76** 4250–3
[2] Kirilyuk A, Kimel A V and Rasing Th 2010 *Rev. Mod. Phys.* **82** 2731–84
[3] Kirilyuk A, Kimel A V and Rasing Th 2013 *Rep. Prog. Phys.* **76** 026501
[4] Malinowski G, Dalla Longa F, Rietjens J H H, Paluskar P V, Huijink R, Swagten H J M and Koopmans B 2008 *Nat. Phys.* **4** 855
[5] Melnikov A, Razdolski I, Wehling T O, Papaiannou E Th, Roddatis V, Fumagalli P, Aktsipetrov O, Lichtenstein A I and Bovensiepen U 2011 *Phys. Rev. Lett.* **107** 076601
[6] Eschenlohr A, Battiato M, Maldonado P, Pontius N, Kachel T, Holldack K, Mitzner R, Föhlisch A, Oppeneer P M and Stamm C 2013 *Nat. Mater.* **12** 332–6
[7] Bergeard N, Hehn M, Mangin S, Lengaigne G, Montaigne F, Lalieu M L M, Koopmans B and Malinowski G 2016 *Phys. Rev. Lett.* **117** 147203
[8] Battiato M, Carva K and Oppeneer P M 2010 *Phys. Rev. Lett.* **105** 027203
[9] Battiato M, Carva K and Oppeneer P M 2012 *Phys. Rev.* B **86** 024404
[10] Rudolf D *et al* 2012 *Nat. Commun.* **3** 1037
[11] Turgut E *et al* 2013 *Phys. Rev. Lett.* **110** 197201
[12] Schellekens A J, Kuiper K C, de Wit R R J C and Koopmans B 2014 *Nat. Commun.* **5** 4333
[13] Savoini M *et al* 2014 *Phys. Rev.* B **89** 140402
[14] Koopmans B, Malinowski G, Dalla Longa F, Steiauf D, Fähnle M, Roth T, Cinchetti M and Aeschlimann M 2010 *Nat. Mater.* **9** 259–65
[15] Schellekens A J, de Vries N, Lucassen J and Koopmans B 2014 *Phys. Rev.* B **90** 104429
[16] Khan S, Holldack K, Kachel T, Mitzner R and Quast T 2006 *Phys. Rev. Lett.* **97** 074801
[17] Holldack K *et al* 2014 *J. Synchrotron Radiat.* **21** 1090
[18] Stamm C *et al* 2007 *Nat. Mater.* **6** 740–3
[19] Chen C T, Idzerda Y U, Lin H-J, Smith N V, Meigs G, Chaban E, Ho G H, Pellegrin E and Sette F 1995 *Phys. Rev. Lett.* **75** 152
[20] Carva K, Legut D and Oppeneer P M 2009 *Europhys. Lett.* **86** 57002
[21] Windt D L 1998 *Comput. Phys.* **12** 360–70
[22] Eschenlohr A, Battiato M, Maldonado P, Pontius N, Kachel T, Holldack K, Mitzner R, Föhlisch A, Oppeneer P M and Stamm C 2014 *Nat. Mater.* **13** 102–3
[23] Zhukov V P, Chulkov E V and Echenique P M 2006 *Phys. Rev.* B **73** 125105
[24] Kaltenborn S and Schneider H C 2014 *Phys. Rev.* B **90** 201104
[25] Knorren R, Bennemann K H, Burgermeister R and Aeschlimann M 2000 *Phys. Rev.* B **61** 9427–40
[26] Schmidt A B, Pickel M, Wiemhöfer M, Donath M and Weinelt M 2005 *Phys. Rev. Lett.* **95** 107402
[27] Andres B, Weiss P, Wietstruk M and Weinelt M 2015 *J. Phys.: Condens. Matter* **27** 015503
[28] Wieczorek J, Eschenlohr A, Weidtmann B, Rösner M, Bergeard N, Tarasevitch A, Wehling T O and Bovensiepen U 2015 *Phys. Rev.* B **92** 174410
[29] Razdolski I, Alekhin A, Ilin N, Meyburg J P, Roddatis V, Diesing D, Bovensiepen U and Melnikov A 2017 *Nat. Commun.* **8** 15007
[30] Chen J, Wieczorek J, Eschenlohr A, Xiao S, Tarasevitch A and Bovensiepen U 2017 *Appl. Phys. Lett.* **110** 092407
[31] Belien P, Schad R, Potter C D, Verbanck G, Moshchalkov V V and Bruynseraede Y 1994 *Phys. Rev.* B **50** 9957–62
[32] Zahn P, Binder J, Mertig I, Zeller R and Dederichs P H 1998 *Phys. Rev. Lett.* **80** 4309–12
[33] Bonetti S, Hoffmann M C, Sher M-J, Chen Z, Yang S-H, Samant M G, Parkin S S P and Dürr H A 2016 *Phys. Rev. Lett.* **117** 087205